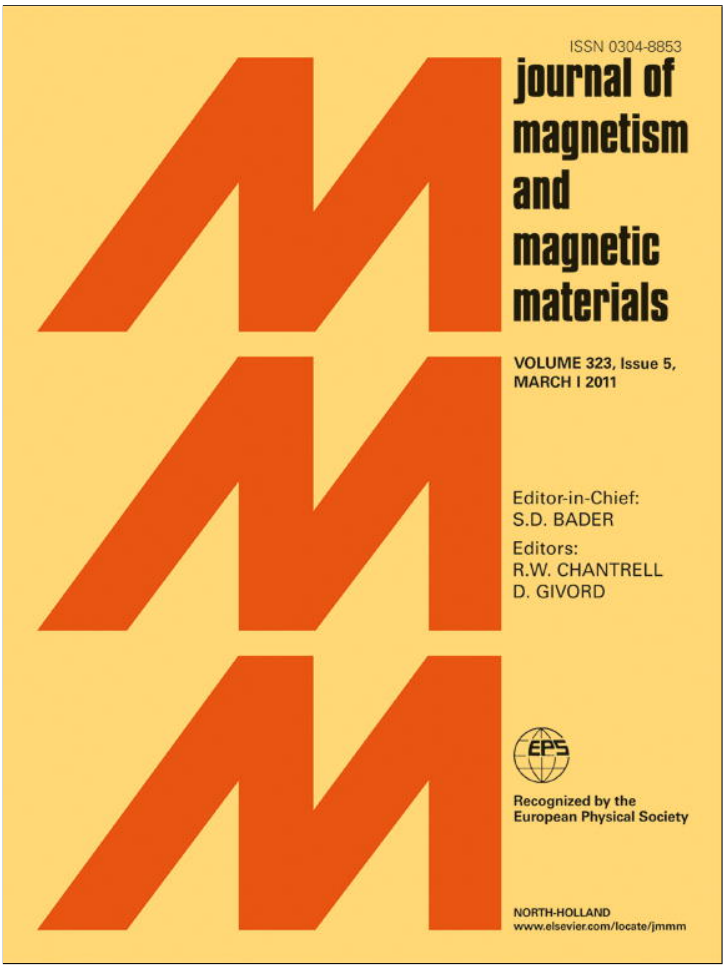

Journal of Magnetism and Magnetic Materials 323 (2011) 400–404

Contents lists available at ScienceDirect

Journal of Magnetism and Magnetic Materials

journal homepage: www.elsevier.com/locate/jmmm

Structural transformations of $Fe_{81}B_{13}Si_4C_2$ amorphous alloy induced by heating

Dragica M. Minić [a,*], Dušan M. Minić [b], Tomáš Žák [c], Pavla Roupcová [c], Bohumil David [c]

[a] Faculty of Physical Chemistry, University of Belgrade, Belgrade, Serbia
[b] Military Technical Institute in Belgrade, Serbia
[c] Institute of Physics of Materials, Academy of Sciences of the Czech Republic, v.v.i. Žižkova 22, 616 62 Brno, Czech Republic

ARTICLE INFO

Article history:
Received 3 July 2010
Received in revised form
21 September 2010

Keywords:
Amorphous material
Metallic glass
Metal and alloy
Phase transition
Thermal analysis
Mössbauer spectrum
X-ray diffraction

ABSTRACT

Thermal stability and crystallization of the $Fe_{81}B_{12}Si_4C_2$ alloy were investigated in the temperature range 25–700 °C by the XRD and Mössbauer analysis. It was shown that on heating the as-prepared amorphous $Fe_{81}B_{12}Si_4C_2$ alloy undergoes thermal stabilization through a series of structural transformations involving the process of stress-relieving (temperature range 200–400 °C), followed by a loss of ferromagnetic properties (Curie temperature at 420 °C) and finally crystallization (temperature range 450–530 °C). The process of crystallization begins by formation of two crystal phases: Fe_3B and subsequently Fe_2B, as well as a solid solution α-Fe(Si). With increase in annealing temperature, the completely crystallized alloy involved only two phases, Fe_2B and solid solution α-Fe(Si).

XRD patterns established a difference in phase composition and size of the formed crystallites during crystallization depending on the side (fishy or shiny) of the ribbon. The first nuclei of the phase α-Fe_3Si were found on the shiny side by XRD after heat treatment even at 200 °C but the same phase on the fishy side of ribbon was noticed after heat treatment at 450 °C. The largest difference between the contact and free surface was found for the Fe_2B phase crystallized by heating at 700 °C, showing the largest size of crystallites of about 130 nm at 700 °C on the free (shiny) surface.

1. Introduction

Amorphous alloys are materials obtained by rapid quenching of the melt at a cooling rate of about 10^5–10^6 K s^{-1} in conditions where crystallization is suppressed [1]. The soft magnetic amorphous alloys are based on the ferromagnetic elements Fe, Co and Ni, containing the glass forming elements Si, B, C and P. The most stable amorphous alloys contain about 80 at% of transition metals (ferromagnetic component) and about 20 at% of metalloid elements (glass forming component) [2]. From a practical point of view, these materials, compared with the crystalline materials, possess a series of advantages, such as magneto-crystalline isotropy, high magnetic softness combined with high mechanical hardness, high mechanical strength, low ribbon thickness and high electrical resistivity, providing excellent soft magnetic material properties for high frequency applications involving very low losses [3–9]. The amorphous alloys are metastable materials and elevated temperature as well as prolonged performance could induce the process of change in their microstructure [10]. The new formed microstructure involves nanocrystals about 10 nm in size embedded in an amorphous matrix possessing soft magnetic properties superior to the amorphous and conventional crystalline magnetic alloys of the same composition [8,11]. However, crystallization of amorphous alloys can provoke the formation of a number of metastable crystalline phases as well as deterioration of their advanced properties, making them effective for only a single use [9,12,13].

Therefore, knowledge of thermal stability, pressure effects, surface effects, microstructure, kinetics of crystallization, as well as composition effects is of great interest for technological applications of amorphous and nanostructured materials [3].

In our previous papers [14–16], research of isothermal and non-isothermal crystallization behavior, and kinetics and mechanism of crystallization of α-Fe from the $Fe_{81}B_{13}Si_4C_2$ amorphous ribbon produced by melt-spinning were reported. Based on the results of DSC and X-ray diffraction analysis (XRD), and on the calculated crystallization parameters ($m=3$; $s=1$), we concluded that primary crystallization of the α-Fe phase in an amorphous matrix occurs through bulk nucleation and three-dimensional growth of nuclei growing at a constant rate [14]. It was established that the kinetic parameters of transformation did not change with degree of crystallization α in the range 0.1–0.7.

* Corresponding author. Tel.: +381 11 3336 689.
E-mail address: dminic@ffh.bg.ac.rs (D.M. Minić).

0304-8853/$ - see front matter © 2010 Elsevier B.V. All rights reserved.
doi:10.1016/j.jmmm.2010.09.027

Also, it was established that primary crystallization of the α-Fe phase from an amorphous alloy cannot be described by the Johnson–Mehl–Avrami (JMA) model, which is usually used for the description of crystallization involving a stage of nucleation, as well as a stage of growth of nuclei. Rather it can be described by the Šesták–Berggren autocatalytic model with the kinetic triplet E_a=349.4.0 kJ mol^{-1}, ln A=50.76 and $f(\alpha)=\alpha^{0.72}(1-\alpha)^{1.02}$ [15]. By correlation of data of the DSC analysis and X-ray diffraction techniques with measurements of electric and magnetic properties very sensitive to structural changes we investigated why the conditions for validity of the JMA model are not fulfilled. It was found that a complex crystallization process involved at least two overlapping steps, which appeared as one sharp slightly asymmetrical crystallization peak on the DSC curve [16]. That could mean that the entire nucleation process did not take place during the early stage of the transformation and became negligible afterward. In this case, the crystallization rate is not defined just by temperature but also depends on previous thermal history of the alloy. That could mean that the process of crystallization is complex, involving crystallization of more than one phases occurring almost at the same time. Therefore, for better understanding of the process of crystallization of the $Fe_{81}B_{13}Si_4C_2$ amorphous alloy in this paper we have correlated the Mössbauer spectra with thermal and XRD analysis of both (shiny and fishy) sides of the amorphous ribbon.

2. Experimental procedure

The ribbon shaped samples of the $Fe_{81}B_{13}Si_4C_2$ amorphous alloy were obtained using the standard procedure of rapid quenching of the melt on a rotating disc (melt-spinning). The obtained ribbon was 2 cm wide and 35 μm thick.

The thermal stability of amorphous alloy was investigated by differential scanning calorimetry (DSC) in a nitrogen atmosphere using SHIMADZU DSC-50 analyzer. In this case, a sample weighing several milligrams was heated in a DSC cell from room temperature to 650 °C in a stream of nitrogen with nitrogen flow rate of 20 ml min^{-1} and at the heating rate of 30 °C min^{-1}.

The temperature induced processes were studied also using a thermomagnetic scan, where the sample is heated, annealed and then cooled in a vacuum furnace at a low magnetic field of 4 kA m^{-1} and its magnetic moment is monitored. Both heating and cooling rates were 4 K min^{-1}, and the dwell time at the maximum temperature of 800 °C was 30 min. These results were used to determine temperatures suitable for intermediate subsequent annealing followed by Mössbauer and X-ray measurements.

Mössbauer spectra were taken in the standard transmission geometry using a ^{57}Co(Rh) source at room temperature. Calibration was done against the α-Fe foil data. For spectra fitting and decomposition, the "CONFIT" program package was used [17].

The X-ray diffraction (XRD) patterns were recorded on an X'Pert PRO MPD diffractometer from PANalytical with CoKα radiation operated at 40 kV and 30 mA. For routine characterization diffraction data was collected in the range of 2θ Bragg angles (15–135°, step 0.008°). All XRD measurements were done with solid samples in the form of a ribbon at ambient temperature. For the qualitative determination of phase composition of the crystallized alloy samples the JCPDS-PDF database was used. For a quantitative analysis and determination of crystallite size the TOPAS V3 general profile and structure analysis software for powder diffraction data was used (Bruker AXS, general profile and structure analysis software for powder diffraction data, Karlsruhe, 2005). This software enables full handling of the instrument geometry and the instrument profile parameters [18]. The quality of refinement progress was controlled by monitoring the fit parameter R_{wp}, goodness of fit (GOF) and the Durbin–Watson factor.

3. Results and discussion

The thermal stability alloy was investigated by thermal analysis using differential scanning calorimetry (DSC). Fig. 1 shows the continuous DSC curve obtained during heating at heating rate β=30 K min^{-1}.

This DSC curve involves series of endo- and exo-peaks in the temperature range 200–560 °C corresponding to a stepwise process of thermal stabilization of alloy. The broad, poorly formed peaks in the temperature range 200–400 °C, corresponding to the stress-relieving transformation at the temperatures, are followed by an endothermic hump at 420 °C corresponding to the Curie temperature and a short super-cooled liquid region, and a sharp exothermic crystallization peak at 539.8 °C. The enthalpy of crystallization was found to be 87.25 J/g.

The appearance of the thermomagnetic curve (Fig. 2) reflects changes in the material magnetic moment. It is sensitive to

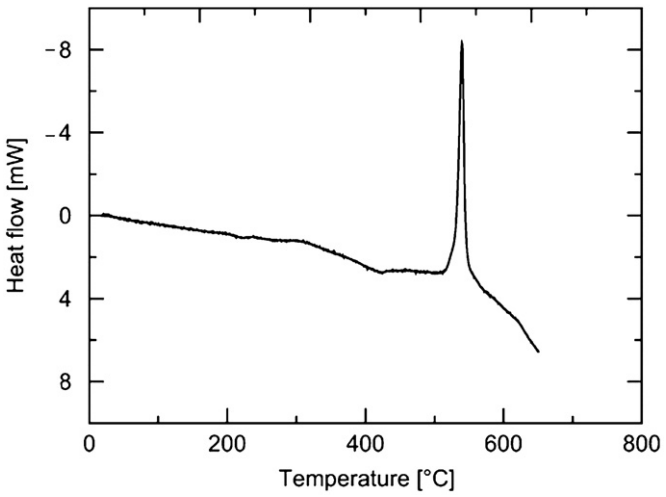

Fig. 1. DSC curve of the as-prepared alloy at a heating rate of 30 °C min^{-1}.

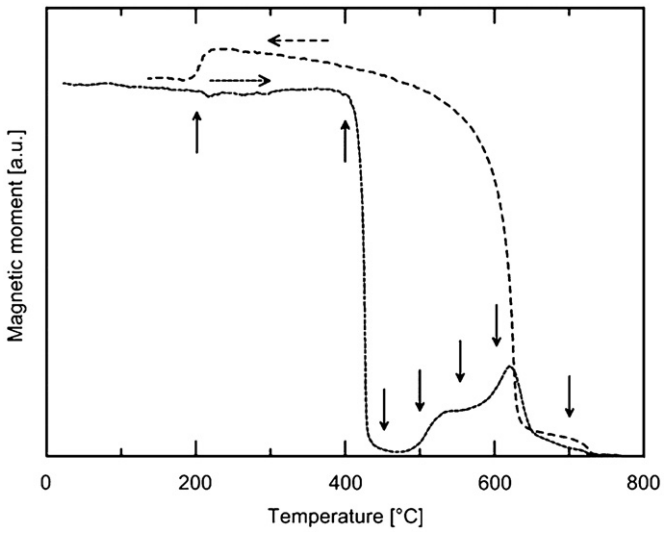

Fig. 2. Thermomagnetic curves for increasing (dotted line) and decreasing (dashed line) temperatures; vertical arrows show the annealing temperatures for Mössbauer and XRD measurements.

changes in atomic magnetic characteristics caused by phase or structural transitions. The most pronounced change represents the Curie point (T_c=420 °C), where magnetization of the appropriate phase drops to almost zero, because the magnetic interaction cannot resist thermal motion any more. The difference between branches for rising and sinking temperatures demonstrates the irreversibility of the whole thermal process. Annealing destroys phases of the as-prepared material while during cooling new and different structures are generated (see below), being characterized by different critical temperatures. Annealing at the temperature near 200 °C is sometimes called stress-relieving and usually enhances properties of the amorphous material. The following sequence of temperatures helps us to understand the process of crystallization and constitution of its products.

The amorphous ribbon in the as-prepared state was also repeatedly vacuum-annealed for 30 min at temperatures marked on the graph with thermomagnetic curves (Fig. 2). In our further investigations, the indicated temperatures of 200, 400, 450, 500, 550, 600 and 700 °C were chosen to examine main features of the thermal process.

In Fig. 3, the spectra illustrate the capability through the Mössbauer effect in distinguishing between individual iron containing phases differing in their structure. Broad-line components are typical for the amorphous volume of the as-prepared sample, while the sharp lines characterize the crystalline structure with well defined position of atoms. This results from the thermally induced crystallization process during annealing of the sample. Computer processing of Mössbauer spectra (Fig. 3) yielded intensities I of components, their hyperfine inductions B_{hf}, isomer shifts δ and quadrupole splitting σ [19]. The contents of the iron containing phases are given to be proportional to the relative areas of the corresponding spectral components (Table 1). However, the exact quantification of the phase contents could be done only when possible differences in values of the Lamb–Mössbauer factors were considered.

The tentative phase analysis showing the quantitative behavior of the crystallization process (Table 1) is based predominantly on Mössbauer results (Fig. 3). In the as-prepared state there is the amorphous structure having a high-field and a low-field component accompanied by a small amount of α-Fe(Si) solid solution and a FeB phase. Moving along the temperature axis, according to the sequence of XRD measurements, the optimum amorphous structure is really near 200 °C, although the Mössbauer spectroscopy shows an appearance of a small amount of α-iron containing an intermediate phase of the crystallization process at this temperature. Mössbauer phase analysis reveals the α-Fe(Si) solid solution and the Fe_2B phase to be the most important final crystallization products. The amount of iron atoms in paramagnetic positions is almost below the sensitivity threshold. Besides α-iron, the next distinctive intermediate phase is Fe_3B, detected initially at 450 °C and predominantly at 500 °C. The content of silicon in the α-Fe(Si) solid solution seems to be about 9 at%, which is not far from the value of 7 at% published in Ref. [20].

The simple qualitative data gained from XRD diffractograms (Fig. 4) was very useful, and mutual consistency of Mössbauer and XRD measurements was essential. The XRD patterns were able to show the difference between the shiny (free) and lusterless fishy (contact) surfaces of the ribbon. The known fact that the free (shiny) surface has stronger tendency to crystallize because of its

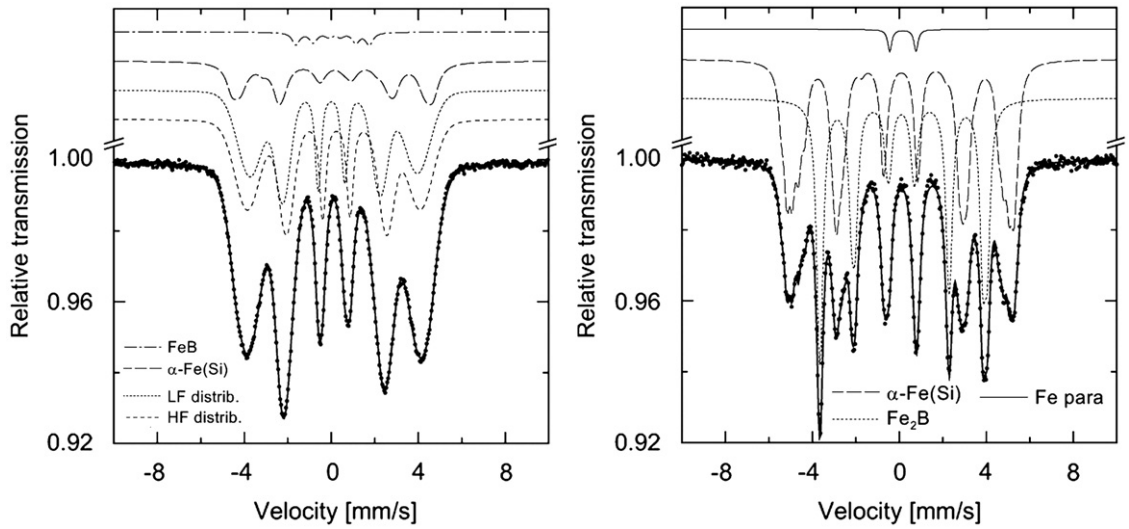

Fig. 3. Mössbauer spectra of the as-prepared material (left) and of the material after final annealing at 700 °C (right), including components of iron containing phases. LF and HF denote low- and high-field components of distributed spectra gained from the amorphous phase, respectively.

Table 1
Mössbauer tentative phase analysis (distribution of Mössbauer iron atoms among phases).

Annealing temperature (°C/30 min)	Amorphous	α-Fe(Si)	Fe_2B	Fe_3B	FeB	α-Fe	Fe para
As-prepared alloy	0.95	0.03	–	–	0.02	–	–
200	0.94	0.02	–	–	0.02	0.02	–
450	0.83	0.14	–	0.03	–	–	–
500	–	0.42	0.42	0.15	–	–	0.01
550	–	0.52	0.47	–	–	–	0.01
600	–	0.54	0.45	–	–	–	0.01
700	–	0.55	0.44	–	–	–	0.01

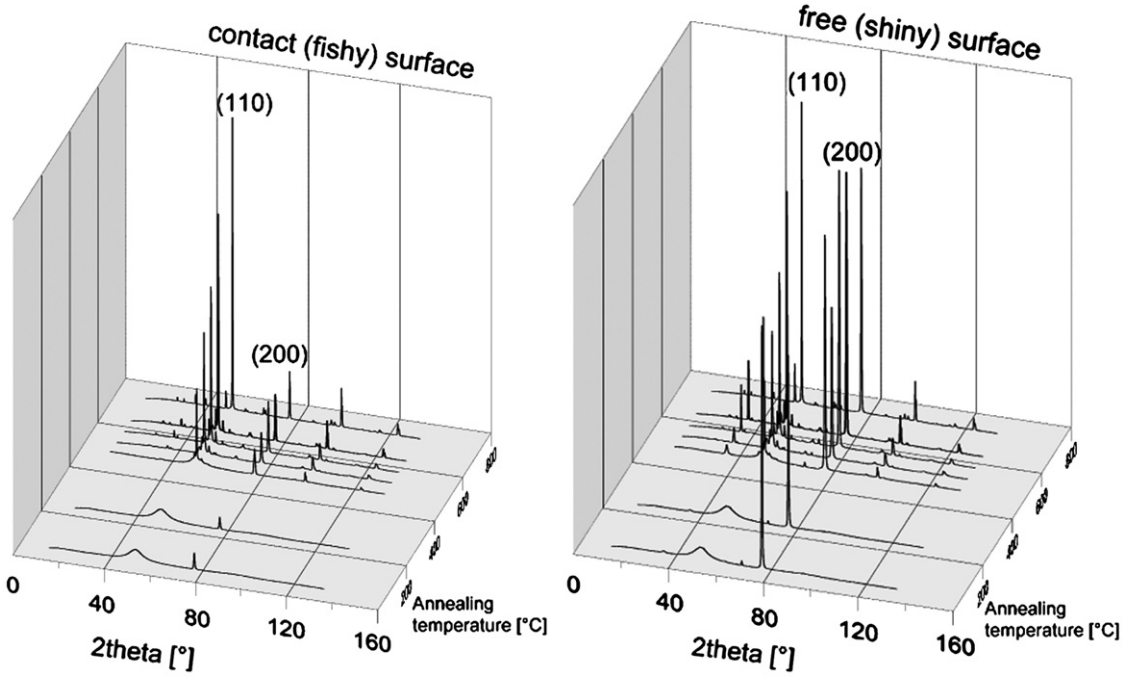

Fig. 4. XRD spectra of the contact (left) and free surface (right). Scaling of intensity axis is the same for both graphs.

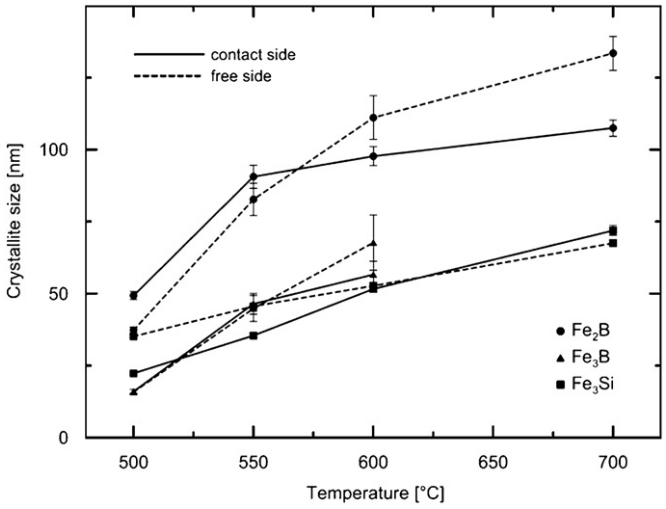

Fig. 5. Growth of crystallite size with temperature determined by line profile analysis.

slightly slower cooling rate is evident in the results, and the narrow temperature range of formation of two different phases in similar amounts can be recognized.

The XRD measurement determined the difference in phase composition during crystallization depending on the side (fishy or shiny) of the ribbon (Fig. 4). The first nucleated phase, α-Fe_3Si, was found on the shiny side by XRD after heat treatment at 200 °C (Fig. 5). The same phase on the fishy side of ribbon was detected after the next step of crystallization (at 450 °C). The slower crystallization of this phase on the fishy side is in agreement with the mean coherent length, which is one-half the size at temperatures up to 600 °C.

The mean coherent length (sometimes called crystalline size), as derived from the Rietveld calculation, markedly increases between the annealing steps at 500 and 700 °C for all important phases. The highest value of about 130 nm at 700 °C is exhibited by the Fe_2B phase on the free (shiny) surface. For this phase and this temperature, the largest difference between contact and free surface can also be observed.

4. Conclusion

XRD pattern and Mössbauer tentative phase analysis revealed the amorphous state of the as-prepared alloy. Heating the as-prepared amorphous $Fe_{81}B_{12}Si_4C_2$ alloy causes it to undergo the processes of stabilization through a series of structural transformations involving the process of stress-relieving (temperature range of 200–400 °C) followed by loss of ferromagnetic properties at the Curie temperature (420 °C), and finally the process of crystallization (temperature range of 450–530 °C). The process of crystallization for the alloy annealed at 500 °C involves the formation of two crystal phases: Fe_3B (15%) and, originating from it, Fe_2B (42%) as well as a solid solution α-Fe(Si) (42%). With increase in annealing temperature, the less stable Fe_3B phase disappeared, giving rise to the formation of α-Fe(Si), so the completely crystallized alloy involves only two phases, Fe_2B (44%) and the solid solution α-Fe(Si) (55%). The percentage of phase is taken from the relative areas of the corresponding Mössbauer spectral components.

XRD patterns established the difference in phase composition during crystallization depending on the side (fishy or shiny) of the ribbon. The first nucleated phase, α-Fe_3Si, was found on the shiny side by XRD after heat treatment at 200 °C, but the same phase on the fishy side of the ribbon was detected only after heat treatment at 450 °C. The slower crystallization of this phase on the fishy side is in agreement with one-half the size of the mean coherent length at temperatures up to 600 °C. The largest difference between the contact and free surface was found for the Fe_2B phase crystallized by heating at 700 °C, exhibiting the largest size of crystallites of about 130 nm at 700 °C on the free (shiny) surface.

Acknowledgements

The research has been supported by the Ministry of Science and Environmental Protection of Serbia, under the Project 142025, by grants 102/01/1335/B and 202/01/0668 of the Grant Agency of the Czech Republic and by the Czech Ministry of Education, Youth and Sports, Project 1M0512.

References

[1] D.M. Minić, Sci. Sintering 38 (2006) 83–92.
[2] M. Iqbal, J.I. Akhter, H.F. Zhang, Z.Q. Hu, J. Non-Cryst. Solids 354 (2008) 5363.
[3] K. Biswas, S. Ram, L. Schultz, J. Eckert, J. Alloys Compd. 397 (2005) 104.
[4] N. Cowlam, J. Non-Cryst. Solids 205–207 (1996) 567.
[5] D.S. Santos, R.S. de Biasi, J. Alloys Compd 335 (2002) 266.
[6] T. Gloriant, S. Surinach, M.D. Baro, J. Non-Cryst. Solids 333 (2004) 320.
[7] J.S. Blazquez, M. Millan, C.F. Conde, V. Franco, A. Conde, S. Lorenzo-Perez, J. Non-Cryst. Solids 354 (2009) 5135.
[8] D.R. dos Santos, D.S. dos Santos, J. Non-Cryst. Solids 304 (2002) 56.
[9] D.R. dos Santos, D.S. dos Santos, Mater. Res. 4 (2001) 47.
[10] M. Miglierini, J. Non-Cryst. Solids 354 (2008) 5093.
[11] A.A. Soliman, S. Al-Heniti, A. Al-Hajry, M. Al-Assiri, G. Al-Barakati, Thermochim. Acta 413 (2004) 57.
[12] H.F. Li, R.V. Ramanjujan, Mater. Sci. Eng. A 375 (377) (2004) 1087.
[13] J. Bednarick, R. Nicula, M. Stir, E. Bukel, J. Magn. Magn. Mater. 316 (2007) e823.
[14] D.M. Minić, A. Maričić, B. Adnađević, J. Alloys Compd. 473 (2009) 363.
[15] D.M. Minić, B. Adnađević, Thermochim. Acta 474 (2008) 41.
[16] D.M. Minić, D.G. Minić, A. Maričić, J. Non-Cryst. Solids 355 (2009) 2503.
[17] T. Žák, Mössbauer Spectroscopy in Material Science, in: M. Miglierini, D. Petridis (Eds.), NATO Science Series, Kluwer, Dordrecht1999, p. 385.
[18] A.X.S. Bruker, TOPAS V3: general profile and structure analysis software for powder diffraction data, Karlsruhe, 2005.
[19] T. Žák, Y. Jirásková, Surf. Interface Anal. 38 (2006) 710.
[20] N. Saegusa, A.H. Morrish, Phys. Rev. B 26 (1982) 305.